CHARLES UNIVERSITY

Faculty of Science

Course of Study: Chemistry

Subject: Analytical Chemistry

Bc. Shannelle Diana Habániková

APPLICATION OF QUANTITATIVE ELECTRON PARAMAGNETIC RESONANCE (EPR) AND COMMERCIALLY AVAILABLE EPR STANDARDS FOR ELECTROCHEMICAL STUDY OF THE SUBSITUTED TETRATHIAFULVALENE OXIDATION

Použití kvantitativní elektronové paramagnetické rezonance (EPR) a komerčně dostupných EPR standardů při studiu elektrochemické oxidace substituovaných tetrathiafulvalenů

Master Thesis

Supervisor of the master thesis: Dr. rer. nat. Ing. Ján Tarábek

Advisor: Doc. RNDr. Ivan Jelínek, Ph.D.

Prague 2019

Prohlášení

Prohlašuji, že jsem tuto závěrečnou práci zpracoval/a samostatně a že jsem uvedl/a všechny použité informační zdroje a literaturu. Tato práce ani její podstatná část nebyla předložena k získání jiného nebo stejného akademického titulu. Jsem si vědom toho, že případné využití výsledků, získaných v této práci, mimo Univerzitu Karlovu je možné pouze po písemném souhlasu této univerzity.

V Praze 17. května 2019

Abstract

Tetrathiafulvalene derivatives are remarkable molecules, with various application, reported relatively recently. The radical cation of these compounds has very interesting optical, electronic, electrocatalytic superconducting and magnetic properties that have been intensively studied recently. Quantitative in-situ EPR voltammetric spectroelectrochemistry studies of 2–(2–hydroxyethylsulfanyl)–3–(benzylsulfanyl)–6,7–bis(octadecylsulphanyl)tetrathiafulvalene (TTF-Der3) have been carried out with the aim to confirm the oxidation sites, follow–up reactions (after the first electron transfer), and electrochemical behaviour. The diffusion process was confirmed by the dependence of current on the square root of the scan rate. It was claimed that the ratio of the number of generated radicals to transferred charge (electrons) for two representative TTF derivatives was determined to 5.5:500 for and 7:500 for TTF, indicating the follow–up reactions. Experiments were performed using the commercially available EPR standards, calibrated for this method (experimental setup). The latter was validated by quantitative EPR with standard 4–hydroxy–2,2,6,6–tetramethylpiperidin–1–oxyl radical concentration ($1{\cdot}10^{-4}\,\mathrm{mol\,dm^{-3}}$). For the ratios the confidence interval was reported for the first time for TTF-Der3 it was $0.011{\pm}0.001$ and $0.014{\pm}0.001$ for TTF. For the future experiments different solvents, test concentration dependencies and additional substituents with donor/acceptor features related to TTF-core, will be used in order to study the follow–up reactions and intramolecular reactions more deeply. Finally, the concentration of paramagnetic centers in the manganese standard should be dicsussed with the manufacturer of the EPR standard to match lower analyte concentrations.

Keywords

Quantitative EPR (ESR) spectroelectrochemistry, Cyclic voltammetry, Charge transfer complexes, Tetrathiafulvalene

Abstrakt (česky)

Deriváty tetrathiafulvalenu jsou pozoruhodné molekuly, objevené a zkoumané poměrně nedávno. Radikál kationt těchto sloučenin má optické, elektronické, elektrokatalytické, supravodivé a magnetické vlastnosti, kvůli kterým je v poslední době intenzivně studován. Kvantitativní in-situ EPR voltametrické spektroelektrochemické studie 2- (2-hydroxyethylsulfanyl) -3- (benzylsulfanyl) -6,7-bis (oktadecylsulfanyl) tetrathiafulvalenu (TTF-Der3) byly provedeny, aby potvrdily pozici oxidačních míst, následných reakcí (po přenosu elektronu) a elektrochemického chování. Byl potvrzen difúzní proces závislostí proudu na druhé odmocnině rychlosti skenu. Dále bylo potvrzeno, že poměr počtu generovaných radikálů k přenesenému náboji (elektronům) pro dva reprezentativní TTF deriváty byl stanoven na 5,5:500 pro TTF-Der3 a 7:500 pro TTF. To poukazuje na následné reakce s vyšší tendenci pro TTF-Der3. Experimenty byly provedeny pomocí komerčně dostupného standardu Manganu pro EPR, kalibrovaném pro tuto metodu (experimentální uspořádaní). Posledně jmenovaná byla validována pomocí kvantitativní EPR s použitím standardu (radikálu): 4–hydroxy–2,2,6,6–tetramethylpiperidín–1–oxyl s koncentrací $1{\cdot}10^{-4}\,\mathrm{mol\,dm^{-3}}$. Pro poměr počtu částic byl také poprvé uveden experimentálně stanovený interval spolehlivosti u TTF-Der3, který činil (0.011 ± 0.001) a (0.014 ± 0.001) pro TTF. Do budoucnosti by byly plánovány experimenty s různými rozpouštědly, koncentrační závislosti analytu a taky větší variace substituentů s donormi/akceptormi (vzhledem k centrálnímu TTF) aby mohly být následné chemické reakce a intramolekulární interakce studovány detailněji. Snížení počtu paramagnetických center Mn-standardu bude konzultováno s výrobcem tak, aby mohly být standardy použity i na mnohem nižším koncentrace analytů.

Klíčová slova

Kvantitativní EPR (ESR) spektroelektrochemie, Cyklická voltametrie, Komplex přenosu náboje, Tetrathiafulvalén

Acknowledgments

I am deeply grateful to my supervisor Dr. rer. nat. Ing. Ján Tarábek, for his willingness and patience, for his detailed and constructive advice and comments and a possibility to work on a very interesting project, where I could learn a lot of priceless knowledge concerning EPR and basic programming. I also want to thank him for helping me with all the R and Python programming language scripts and invaluable support throughout this work. I wish to extend my warmest thanks to Doc. RNDr. Ivan Jelínek, Ph.D. for making this cooperation work. Big thanks belong to all colleagues from the laboratory for their advice and the creation of an excellent working environment. I owe my thanks to my parents, my partner and my closest friends for their loving support during my study, their encouragement and appreciation.

Contents

List of Figures

List of Tables

Chapter 1

Introduction and Aim

Electronic transistors are very important and crucial components in modern electronics for almost a century. In this period of time, they have gone through an intensive development leading to a great information technology boom in a past decade and there is still immense pressure to reach higher and more efficient output on processors and graphics cards. From the 1970s and discovery of organic charge transfer (CT) complexes, molecular electronics has been one of the most interesting and important fields[1]. The properties of charge transfer complex of tetrathiafulvalene (TTF) and tetracyanoquinodimethane (TCNQ) was studied to a large extent by x–ray[2] and infrared spectroscopy[3], or various electrochemical methods[4].

Additionally, it was discovered that various TTF substituents affect the charge transfer complex of tetrathiafulvalene radical cation and TCNQ radical anion[5]. Because this influences the stability and conductivity of a CT complex, it was desirable to investigate and characterize these new structures for "Langmuir-Blodgett"(L–B) organic electronics.

Aim

The aim of this diploma thesis is to determine the basic EPR parameters of novel $TTF^{\bullet+}$ derivatives and confirm oxidation sites, follow–up reactions, spin density and electrochemical behaviour in context with nowadays knowledge. Furthermore, the purpose was to determine the ratio of the number of generated radicals to transferred charge (electrons, by electrochemical way) for two representative TTF derivatives and its confidence interval, by application of commercially available EPR standards. The additional aim in this context was to answer the question whether the last–mentioned standards are applicable for such determination. This was achieved by using in situ simultaneous quantitative EPR spectroscopy with cyclic voltammetry performed under

very specific conditions (e.g. non–aqueous environment). Cyclic voltammetry also with quantitative EPR can detect the presence of subsequent reactions (e.g. dimerization, association) after electron transfer. The data will serve as a knowledge base for the determination of the structure of CT complexes (salts) in L–B layers.

The novelties of this work include the redox properties of new structures for the "L–B" organic microelectronics. Furthermore, application and validation of commercially available EPR standards and determination of confidence interval for the ratio of generated number of radicals to the number of transferred electrons, which was not reported up to now.

The entire experimental work as well as most of the data treatment and analysis were performed at the Institute of Organic Chemistry and Biochemistry in Prague

Chapter 2

Knowledge Base

The theoretical part covers all important background knowledge related to the topic. The first part is devoted to the general characteristics of studied chemicals, from their structure to their physicochemical properties, including charge-transfer complexes, association (dimerization) and redox properties. The second part gives a small insight into the current knowledge and possibilities of their chemical, electrochemical and finally EPR spectroscopic.

2.1 History and applications

When in 1915 AT&T conducted their first transcontinental telephone system, the need for signal amplification grew, and together with Bell Labs, they started Solid State Physics group that subsequently invented the first transistor in 1947, specifically by Bardeen, Brattain and Shockley (awarded the Nobel Prize in physics 1956) [6]. Then, in 1958 Jack Kilby from Intel developed the first integrated circuit (awarded the Nobel prize in physics 2000). In 1965 another Intel co-founder Gordon Moore stated Moore's law, which asserts that the number of transistors in a dense integrated circuit doubles every two years. He was right because even though the world could not imagine the realization, it was clear that the miniaturization and resource saving is a necessity. One of the solutions to this problem came in the 1970s with the discovery of metallic properties in organic molecules, when interacting in CT complex salt [7]. In 1972, Wudl et al. manifested that the TTF radical cation displays semiconductor behaviour and subsequently in 1972 Ferraris et al. [1] demonstrated that TTF and TCNQ formed a $1:1$ ionic organic salt, a CT complex with exceptional conductivity [7–9]. CT interactions between electron acceptors (TCNQ) and donors (TTF) emerge in augmented optical

and electronic properties [8].

The charge transfer interaction is very relevant to real-world applications. The application of conductive organic substances to electronic appliances is the main interest of current industrial and academic research [8]. These complexes can help in constructing a molecular rectifier or a high electrically conductive system [10].

Donor-acceptor (charge-transfer) complexes have long been a subject of interest. Since the initial works by Mulliken et al. [11], many teams worked on this topic. Recently, they even have attracted attention because of their role in organic solar cells and organic light-emitting diodes [12, 13].

Thanks to the effectivity of the conductive organic salt complex TTF-TCNQ, they are widely used as a biosensor mediator, because in a chemistry nanometre scale, one can control individual atoms and functional groups by synthesis and its structured order make CT easier [14]. The potential range of these biosensors is from $-0.075\,\mathrm{V}$ to $0.300\,\mathrm{V}$ vs. SCE (standard calomel electrode), where it can be used to detect the substrates such as glucose, fructose, lactate, hydrogen peroxide, glutamate, lactulose, biologial purines, dopamine, hypoxanthine, acetylcholine and choline, methanol, sulfite, and formaldehyde.

TTF-TCNQ is also a super catalyst of electrochemical oxidation of amino acids, but special preparation is needed for bioelectrochemical applications to use as a monocrystal or deposited on an electrode surface. This application of CT complexes in bioelectrochemistry is possible thanks to its low toxicity (LD50 TTF $710\,\mathrm{mg\,kg^{-1}}$ LD50 TCNQ $1225\,\mathrm{mg\,kg^{-1}}$ [15] and besides the fact that the monolayer of this salt strengthens mentioned electrocatalytic properties, it has also better contact with the enzymatic active centres [14]. That is why it is a good candidate to be utilized as a nanochip or other macromolecular technologies. The formation of TTF-TCNQ monolayer is achieved by chemical functionalization or electrochemical deposition on carbon nanotubes and these nanosensors possibly have higher response current and bigger active area than the planar or fibre electrodes [14]. Further applications of TTF can be found in extensive reviews by Bryce et al. and Segura et al. [16, 17].

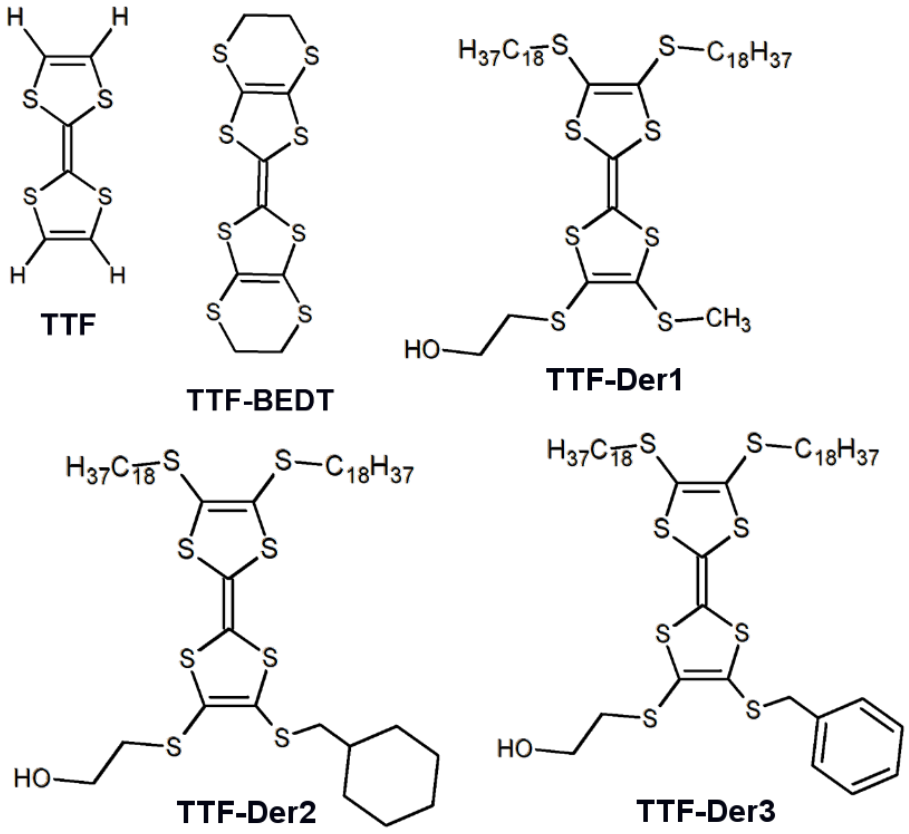

Figure 2.1: The structures of the studied compounds

2.2 Studied substances and their physicochemical properties

TTF and its derivatives belong to organosulphur compounds, they are composed of two heterocyclic circles connected by a double bond, that contains 14 π-electrons in the neutral state. By easy and reversible electrochemical oxidation TTF transitions first to the $TTF^{\bullet+}$ and the further loss of an electron to the TTF^{2+} dication, which also leads to an aromatic character. The ability to behave as a strong electron-donor is preserved by the TTF-unit even when embedded in more complex structures applicable in a variety of applications. TTF and its derivatives act as widely used donor molecule in the field, also due to good chemical stability, usable synthesis, and their outstanding donor properties [10]. The radical cations of studied tetrathiafulvalene form charge transfer complex with the radical anions of TCNQ. The tetramethyltetrathiafulvalene salts (Fabre salts) have superconducting properties used in microelectronics. These complexes can be also applied for construction of Langmuir-Blodgett monolayers for

the organic electronic components (e.g. Organic "Field-effect" Transistors (OFET)). The advantages of OFETs over their inorganic counterparts are light weight, low cost, mechanical flexibility, large-area coverage, and compatibility with plastic substrates [18].

For optimal formation of LB monolayers on air-water interface, amphiphilic TTF derivatives were needed. TTF derivatives with eighteen carbons in the hydrophobic alkyl chain, which is long enough so that they do not form micellar assemblies and are still soluble in water and short enough so that they do not crystalize and therefore are succesful in forming the monolayer. New TTF derivatives were formed by condensation reaction of two monocyclic units with altered structure so that one of the nuclei contains two octadecyl groups representing the hydrophobic moiety and the other end one or two hydrophilic functions with hydroxyl groups [19]. Finally the structures seen in the Figure 2.1 were studied further by CV and EPR. These include TTF, bis(ethylenedithiol)-TTF (BEDT–TTF) and derivatives with octadecyl groups on one side and ehylalcohol residue and (1)methyl, (2) methylcyclohexyl and (3) benzyl substitutes.

TTF derivatives have great properties for acting as semiconducting layers in OFETs: easily synthetized and chemically modified; generally soluble in common solvents and benefit the solution-processable devices; the planar molecular conformation and the strong intermolecular interactions in the solid-state induced by $\pi\cdots\pi$ stacking and S···S interactions; and the good electron donor ability with highest occupied molecular orbital (HOMO) levels close to the work function of usual metallic electrodes, affording little energy barrier for charge injection from metal electrodes into their active layers [18].

They can be used as metallic thin-film electrodes [20], and also as a single crystal layer of OFETs [21]. The ambipolar FET characteristics of devices based on single crystals of organic CT compound $(BEDT-TTF)(F_2TCNQ)$ (F_2TCNQ = 2,5-difluorotetracyano-quinodimethane) was reported. Bourgoin et al. reported the first TTF-based OFET in which the Langmuir–Blodgett layers of TTF derivative with octadecyl was the active channel of a p-type transistor [22].

Similar TTF derivatives were used in a PhD thesis by Akhtar Naureen, where he used ethylenedithiol (EDT) – $TTF(SC_{18})_2$ and found that it forms a stable monolayer only when mixed with long-chain carboxylic acids [23]. To avoid the use of co-surfactants or long alkyl chains he used several strategies to prepare TTF derivatives that have improved film-forming properties(e.g.: Pyridine-containing TTF donors, Azobenzene-containing TTF donors and Metal dithiolate complexes).

2.2.1 Charge transfer complexes and Langmuir-Blodgett monolayers

The landmark result in the history of organic electronics was the discovery of metallic conductivity in the charge transfer salt TTF-TCNQ [8]. There is a huge difference in conductivity between the CT salt and its neutral components, where TTF and TCNQ alone are insulators. In TTF-TCNQ CT complex an intermolecular charge transfer is observed (noncovalent interactions bind the donor and acceptor units, whereas in intramolecular charge transfer, there is at least one covalent bond between the units) [8]. By exposing the TTF monolayer to an acceptor-like TCNQ induces forming of donor-acceptor complexes. Due to this formation, a reduction of the voltammetric peak currents is observed [10]. An electro-donor and an electro-acceptor CT nature are usually examined in 3D solid-phase systems [10]. Langmuir-Blodgett films are 2D highly quality monolayer with the donor-acceptor organization of a CT salt demonstrating interesting conducting and magnetic properties. To illustrate, a covalent TTF-TCNQ dyad features easily accomplished electron transfer with five stable redox states and a very low highest occupied molecular orbital (HOMO) to lowest unoccupied molecular orbital (LUMO) gap. According to Morisson et al. that prepared giant analogues of TTF derivatives, the monolayer stability surprisingly decreased with alkyl chain lenght, which was explained by steric barrier and controlling the interaction of electroactive cores [24].

When the TTF layer is oxidised to the radical cation, the unpaired electron is delocalised in a conduction band. There is an exchange coupling between localized radicals and conduction electrons, which leads to a co-parallel arrangement of spins on the localised radical centres [7]. The performance of organic photovoltaic devices principally depends on the electronic structure at the interface between an electron donor (D) and an acceptor (A) component in both the ground and excited states [13]. In organic light-emitting diodes, ground-state charge transfer between a charge-transport molecule and a molecular dopant that form a D/A complex is observed in a number of instances to greatly facilitate charge injection from an electrode into the charge-transport material [12].

It was also found that metal organic frameworks are amenable to designs that promote good charge transfer among the individual building blocks of TTF [25]. They designed tetratopic ligand of TTF-tetrabenzoate H_4TTFTB to synthetize Zn_2(TTFTB), permanently porpous metal organic framework with high charge mobility.

Studies of the behavior of fatty acid monolayers on the water-air phase interface were addressed in the 1920s by Irving Langmuir and a detailed description of the

monolayer transmission a few years later by Katherine Blodgett. Monolayer therefore, they are referred to as Langmuir-Blodgett (LB) films. In the 1960s Hans Kuhn Much used LB methods to control the position and orientation of functional molecules within complex assemblies, what is now called "supramolecular assembly" [26].

To form monolayers at the air/water interface, the molecules must must have an amphiphilic nature. First approach is to substitute the molecule with hydrophobic groups, or by substituting with both hydrophobic and hydrophilic groups [26].

The TTF-TCNQ dyad has a low electrochemical HOMO-LUMO gap of 0.17 eV and the intramolecular charge transfer is observed in the solutions [26].

2.2.2 Association / Dimerization

In 1972 Ferraris et al. manifested that CT complex of TTF and TCNQ is a narrow band gap semiconductor [1]. Because of the close packing of molecules, it is important to understand intermolecular interactions between conducting form (mixed dimer $(TTF)_2^{\bullet+}$) and the insulating form (radical-cation dimer$(TTF)_2^{2+}$). Unfortunately, because of their low stability, these can be observed just in high concentrations with low temperatures in liquid media [9].

TTF only form radical cation π-dimers under specific conditions and are rather unstable and sensitive complexes, research shows that supramolecular encapsulation increases the association constant for these dimeric species [27]. For this purpose cucurbit[8]uril is used. In order to produce swichable radical dimers, they are usually interlocked in molecules such as cyclobis(paraquat-p-phenylene)$^{4+}$ ring or [2]catennane, these can be then controled by modulation of weak interactions of these molecules [27].

The TTF electronic properties can be modulated by attaching electron-donating or electron-withdrawing substituents. From the EPR and electrochemistry experiments, they deduced a switching mechanism which governs the redox behavior of the [2]catenane $6{\cdot}4\,PF_6$. After the first one-electron wave at +0.55 V, the approximate 70:30 ratio of electronic translational isomers is established. As a consequence of fast equilibration of the redox-stimulated translational motion of the cyclobis(paraquat-p-phenylene)$^{4+}$ ring, only a single one-electron redox process is observed. This one-electron redox process is assigned to the oxidation of two complex TTF derivativess, in the 70:30 ratio measured from EPR. They observed direct converting of the +1 oxidation state to the +4 state in the next oxidation process, which indicates that the +2 and +3 states are not thermodynamically stable intermediates [28].

To stabilize and study TTF dimers, two main strategies are used. Coskun et al. [9]

used the covalent attachment of the TTF to assist in the formation of the dimers, e.g. bistaple tripodal [4]rotaxane [29], and also stabilization of the dimers by host molecules such as cucurbit[8]uril and molecular cages as well as molecular clips. [3]catenane and [3]rotacatenane integrate both of these approaches and can form robust TTF dimers, stabilized mechanically inside the cavity of a tetracationic molecular square [9]. The stability is low and thus the dimers had been observed only in the solid state or in concentrated solutions at low temperatures, where solvents played an important role [30]. In the past decade, several strategies have been developed to enhance this self-binding motif of the and $TTF^{\bullet+}$ radical cations, which include using a rigid macrocycle or cucurbit[8]uril capsule to encapsulate the dimer [31], holding two radical cation units in place with a preorganized framework, e.g. $(TTF)_{21}$–glycol dendrimer [32], and stabilizing the dimer by utilizing mechanical bonding in interlocked systems, as [2]catenane [28] or crown-ethers [33]. Intramolecular arrangement of dimers occurs in polar solvents [30], e.g. acetonitrile, but is weak in chloroform. In 2014 important role of intramolecular hydrogen bonding and solvent was reported by Wang et al. [34]. The intermolecular dimerization stabilized by dodecamethylcarboranate was described by Rosokha et al. in acetone [35]. Another possibility of stabilization is conjugated radical cation dimerization by supramolecular polymers, in which four TTF subunits were connected to the central tetraphenylmethane by the amide or ethynyl linker. These building blocks could self-assemble into stable 3D supramolecular polymers after the TTF units were oxidized to $TTF^{\bullet+}$ [36].

Due to the weakness of non-covalent interactions involved in self–assembling in the liquid solution, the study of TTF aggregates is still a demanding task [37]. Rosokha and Kochi were observing diamagnetic [$TTF^{\bullet+}$-$TTF^{\bullet+}$] dimer and its self-assembling with high concentrations (within a framework of Diploma Thesis it was investigated at a lower concentration from $5{\cdot}10^{-5}\,\mathrm{mol\,dm^{-3}}$) of TTF salt with a large and non-coordinating carboranate anion in a liquid media at room temperature [35]. They also investigated the association of the $TTF^{\bullet+}$ with neutral TTF resulting in the mixed valence [$TTF^{\bullet+}$-TTF] species. The dimerization process is always driven by the cation radical presence, produced by ex situ electrochemical oxidation. To achieve intramolecular activation of neutral TTF is to use a donor—acceptor dyad. TTF is an electron π-donor, which can be linked to an electron acceptor, which show a two-state reversible switching through an intramolecular electron transfer (IET) process as a reaction to external stimuli like light, temperature, electrical field, pressure or solvent [37]. Where one state has a neutral structure and exhibits structure of a zwitterion,

which should activate the dimerization. TTFs connected to stable neutral radicals form "spin-polarized donors" that has exceptional conducting and magnetic qualities.

Magnetic susceptibility and DFT studies of Venneri et al. showed consistency with antiferromagnetic coupling of spins within a TTF-pyr-verdazyl molecule. However, co-parallel alignment of verdazyl spins was achieved by electron hopping within the mixed valence $(\mathrm{TTF-pyr-(2,5-diisopropyl)verdazyl})_2$ diradical cation through antiferromagnetic exchange between the delocalised TTF-based electron and the localised verdazyl $S = 1/2$ spins [7].

2.2.3 Redox properties – Electrochemistry

TTF derivatives are redox-active π-donors regarded as redox chemical sensors or redox-switchable ligands [38]. Because of the fact that the properties depend on the host unit and types of linkers so extended study was devoted to supramolecular chemistry of these compounds.

TTF derivatives exhibit two-step reversible single-electron oxidation, forming radical cation and a dication fragment respectively [39].

Singh et al. studied BEDT-TTF and other TTF derivatives by cyclic voltammetry and found out that most TTF derivatives show two reversible redox waves, with the first half-wave potential ranged from 0.54 V to 0.59 V and the second from 0.93 V to 1.04 V vs. SCE, corresponding to first and second oxidation step [40].

CV study of TTF-crown ether derivatives also exhibited two-step reversible oxidation with the first stpe at 0.48 V and the second step 0.64 V vs. SCE in acetonitrile with 0.1 mol dm^{-3}TBAPF_6 [38].

Step by step oxidation of two adjacent TTF units, firstly forms a mixed-valence dimeric state and the radical is equally shared, and secondly radical cation π-dimer with overlapping single occupied molecular orbitals(SOMO) allows radical spin-pairing [27].

Tan et al. studied oxidation of TTF and reduction of TCNQ in acetonitrile at Pt, Au, glassy carbon and pBDD electrodes by various techniques. However, the contributions of current by double layer charging currents are linearly dependent on the potential scan rate, v, while Faradaic currents are proportional to $v^{1/2}$ resulting in diminished Faradaic-to-background current ratios at high scan rates, which complicates the reliability of fast electron transfer kinetic measurements [41]. Measured midpoint potentials for TTF oxidation at all electrodes vs.ferrocene redox couple was (-0.074 ± 0.002) V.

2.2.4 Redox properties – EPR

There was always demand for super materials with multiple physical properities, such as electrical conductivity and magnetic interactions, spin crossover and magnetism, optical and magnetic properties. These properties were found in metallic CT salt and different types of TTF-containing metallic radical cation salts, with paramagnetic anions were synthetized to study physical phenomena of the interaction between delocalized conduction electrons and localized magnetic moments [17]. Molecular magnetic semiconductors, metals and superconductors based on BEDT-TTF salts with magnetic anions were reviewed by Day and Kurmoo in 1997 [42].

EPR spectroscopy has been used widely in combination with electrochemistry because of its selectivity toward paramagnetic species, and in connection with voltammetric data, spectroelectrochemical experiments have enabled the mechanistic outcome of complex electrochemical reactions [43]. The $TCNQ^{\bullet -}$ and the $TTF^{\bullet +}$ in 1,2-dichloroethane were produced at the water interface by electron transfer from/to the aqueous-phase ferricyanide/ferrocyanide redox couple by applying a potential difference between the two phases with a four-electrode potentiostat. The EPR signal intensi ty (at constant magnetic field) of the resultant organic radicals was monitored during potential step experiments which indicated that the EPR data could be modeled in terms of diffusional transport. The supporting electrolyte, tetrabutylammonium hexafluorophosphate $TBAPF_6$ used in several experiments to avoid problems associated with the photoinduced oxidation of tetraphenylborate derivatives supporting electrolytes. The cell that was used to perform the EPR experiments ia a modified conventional silica flat cell modified so that a counter and reference electrodes can be inserted into opposite ends [43]. We used similar set up in our experiments. Cottrell-type behavior was observed, when the EPR signal intensity (at constant magnetic field) obtained by applying sufficient potential to produce the $TTF^{\bullet +}$ by one-electron transfer across the water/1,2-dichloroethane interface. The EPR signal is a function of time, as expected for a diffusion-controlled heterogeneous electron-etransfer reaction. However, due to high ohmic resistance the design of the cell for optimal spectroscopic performance meant that simultaneously obtained data was of limited value [43].

The EPR spectra of all CT complexes from Singh et al. work show symmetric singlet [40]. Variable temperature ESR spectra of perchlorotriphenylmethyl-TTF derivative dyad in dimethylformamide ($5{\cdot}10^{-5}$ mol dm^{-3}) do not give any signal in the range from 260 K to 350 K demonstrating that the zwitterionic species are completely dimerized producing the stable and EPR-silent π-dimer in conformity with the known trend of the

$TTF^{\bullet+}$ to aggregate in solution forming diamagnetic supramolecular structures [37]. A decreasing trend in g-values on temperature dependence (200 K to 300 K) was observed in all solvents (acetone, CH_2Cl, and acetonitrile) specifically from 2.0030 to 2.0027 in acetonitrile [37].

Additionally EPR spectrum of tetrakis(methylthio)-TTF in CH_2Cl_2 at room temperature, can be simulated with hyperfine couplings to 12 equivalent protons [I = 1/2, $a_{iso}(^1H) = 0.025\,mT$] from methyl groups, four equivalent sulfurs[I = 3/2, $a(^{33}S) = 0.42\,mT$] inside the TTF core, and two equivalent carbon atoms [I = 1/2, $a_{iso}(^{13}C) = 0.58\,mT$] of the central double bond [39].

2.3 Methods

2.3.1 EPR

Magnetic resonance is an important concept used in two spectroscopic chemical procedures, namely Nuclear Magnetic Resonance (NMR) and Electron Paramagnetic Resonance (EPR). Resonance is a condition of strong effective coupling when the two oscillators' frequencies are identical.

EPR spectroscopy, sometimes also called Electron Spin Resonance (ESR) spectroscopy is the most effective method for detection of paramagnetic particles [44]. The paramagnetic effect of atoms and molecules results from an odd number of electrons, which is caused by the presence of a non-zero electronic spin, $S > 0$. The electromagnetic radiation (microwave frequency, GHz) is then absorbed by these substances and that is a necessary condition for EPR spectroscopy.

With the use of EPR spectroscopy it is possible to demonstrate the presence and identify certain particles that contain unpaired electrons. Furthermore, it can provide both spectroscopic and kinetic information about some organic or inorganic compounds and ion radicals. The subjects of study are highly differentiated EPR spectra of paramagnetic systems in solutions [44]. The method is advantageous both in terms of high sensitivity, reactivity and also molecular structure.

History

In 1896, Dutch physicist Zeeman observed the splitting of the frequencies of transition in optical spectra in a static magnetic field. Then in the 1920s, Stern and Gerlach monitored how a beam of silver atoms sent through an inhomogeneous magnetic field

splits into two distinct parts, hinting the angular momentum of electrons and atoms. Then Uhlenbeck and Goudsmit suggested that electrons have the angular momentum. In 1938, Isidor Rabi measured the magnetic resonance absorption of lithium chloride molecules that enabled him to get more detailed information about the structure. After World War II, microwave instrumentation's were much more available so it accelerated the development of EPR. Magnetic resonance electron spin signal was first observed by Soviet physicist Zavoisky in salts including hydrous copper chloride, copper sulfate and manganese sulfate in 1944. The basic theory of magnetic resonance was then proposed by the Oxford group. From then many researchers studied EPR (Cummerow & Halliday and Bagguley & Griffiths). From 1960 to 1980, new techniques like a continuous wave (CV) EPR and pulsed EPR were developed and studied in Bell's laboratories. EPR was usually used for detection of organic free radicals, but from the 1980s, first pulsed EPR spectrometer showed up in the market and was then widely utilized for instance for biological, medical field, and active oxygen. These days, EPR has turned into an adaptable and standard research tool [44].

Basic principle

The energies of electron in the magnetic field $\vec{B}_0$ can be characterized by the mathematical statements summarized in the following lines. Magnetic moment ($\vec{\mu}_{\vec{S}}$) corresponding to the electron spin can be described by Equation (2.1), containing the g-value g_e of an electron ($g_\mathrm{e} = 2.002319$ approximately); Q the charge of the electron; m_e as electron mass and $\vec{S}$ is a vector of spin angular momentum.

$$\vec{\mu}_{\vec{S}} = \vec{\mu}_\mathrm{e} = g_\mathrm{e}\frac{Q_\mathrm{e}}{2m_\mathrm{e}}\vec{S} = -\frac{1}{\hbar}g_\mathrm{e}\mu_\mathrm{B}\vec{S} \tag{2.1}$$

Property called Bohr magneton μ_B, is regarded as the fundamental quantum of magnetic moment of an electron and is defined by Equation (2.2), where Dirac constant $\hbar$ equals to the Planck's constant h divided by 2π and γ_e is the spin magnetogyric ratio of the electron. Corresponding to negative value of elementary charge e divided by double of electron mass.

$$\mu_\mathrm{B} = \frac{e\hbar}{2m_\mathrm{e}} = -\gamma_\mathrm{e}\hbar \approx 9.274{\cdot}10^{-24}\,\mathrm{J\,T^{-1}} \tag{2.2}$$

Similarly, the magnetic moment ($\vec{\mu}_{\vec{I}}$) corresponding to the nuclear spin can be described by Equation (2.3), containing the g-value g_p of a proton ($g_\mathrm{p} = 5.585694$ approximately); m_p as proton mass and $\vec{L}$ is a vector of orbital angular momentum.

$$\vec{\mu}_{\vec{I}} = \vec{\mu}_{\mathrm{p}} = g_p \frac{Q_{\mathrm{e}}}{2m_{\mathrm{p}}} \vec{I} \tag{2.3}$$

The energy of a magnetic moment $\vec{\mu}$ in a magnetic field $\vec{B}_0$ is equal to the scalar product of these two. After substituting the magnetic moment equation we get Equation (2.4), corresponding to the energy of α spins and Equation (2.5), corresponding to the energy of β spins:

$$E_\alpha = \frac{1}{2} g_{\mathrm{e}} \mu_B B_0 \tag{2.4}$$

$$E_\beta = -\frac{1}{2} g_{\mathrm{e}} \mu_B B_0 \tag{2.5}$$

Electron paramagnetic resonance is the study of molecules and ions containing unpaired electrons by observing the magnetic fields at which they come into resonance with monochromatic radiation. To achieve resonance, the radiation of frequency ν needs to satisfy the resonance condition that is equal to the difference in the energy of α and β states, as seen in Equation (2.6).

$$\Delta E = E_\alpha - E_\beta = g_{\mathrm{e}} \mu_B B_0 = h\nu \tag{2.6}$$

Hyperfine splitting/coupling refers to small shifts and splittings in the energy levels of atoms, molecules, or ions, due to interaction between the magnetic moments arising from the spins of both the nucleus and electrons in atoms an this information is used in structure determination. The number of lines observed in simple EPR spectrum can be calculated from simple equation Equation (2.7). Where I is a nuclear spin and N is a number of equivalent nuclei.

$$2NI + 1 = n_l \tag{2.7}$$

Especially in EPR we track the distance of these lines and that is called the hyperfine splitting constant a and is acquired directly from EPR spectrum. Then **hyperfine interaction constant** A can be derived from a by an Equation (2.8) simply by multiplying it by g_{e} and μ_{B} and is **usualy transferred to** A/h **then in MHz**.

$$A = g_{\mathrm{e}} \mu_B a \tag{2.8}$$

Quantitative in-situ EPR spectroelectrochemistry

In 1999 Neudeck at al. reported new method to get quantitative information on the distribution of the conjugation chain length in polymers [45]. The in-situ combination of quantitative EPR spectroscopy and voltammetry/coulometry is the only direct method to determine the reactivity of radicals. This method was applied in observing reaction mechanisms of polypyrrol and its behaviour during oxidation [46]. They also used cyclic voltammograms to determine the transferred charge and potentials referred to the ferrocene/ferrocenium couple against silver pseudo electrode [47]. The EasySpin program was written in Matlab to simulate EPR spectra easily [48].

2.3.2 Cyclic Voltammetry

In 1922, J. Heyrovsky decided to connect mirror galvanometer to the circuit of electrocapillaries to simplify dependence curves of surface tension on potential and measure the dependence of flowing current on the potential of dropping mercury electrode (DME). This was revolutionary and he soon noticed that various metal ions cause an increase of current at specific potentials and this signal forms a wave, while its height is directly proportional to the concentration of the ion. In 1924, together with Japanese coworker M. Shikatou developed an automatized apparatus that could record dependence of current on potential automatically and named it polarograph and the technique polarography. That is why the Nobel Prize for chemistry in 1959 was awarded to J. Heyrovsky [49].

Cyclic voltammetry (CV) is the most diverse technique that is utilized and it has very good sensitivity and selectivity among electrochemical techniques. We can monitor an oxidation/reduction current that occurs at a particular voltage, which is dependent on the properties of the analytes. It is also the cutting edge study of electron transfer. This method provides information about the consequences of electron transfer, and kinetics, and thermodynamics of this reaction. The real advantage is that not only information about concentration is acquired, but also information about its kinetics and therefore about the mechanism of electrochemical reaction, which leads to a better understanding of electrochemical properties of analytes [50].

Basic principle

Voltammetric techniques are methods used to monitor the dependence of current passing through the polarizable working electrode immersed in the analyzed solution.

A potential ramp or potential shift is utilized and it monitors the resulting current between the working and counter electrode. When oxidation is conducted, a peak current I_p is observed, because of a loss of an electron, observed as an oxidation peak that is proportional to the concentration c, then after a time t, the potential E is reversed and a reduction peak is observed.

CV is a potential dynamic electrochemical measurement technique. The working electric potential increases and decreases linearly with time, from E_0, initial potential, to E_1, vertex potential, and back.

As the potential program proceeds, the dependence of current on potential is measured, and we can follow the rise of the capacitive current, then innate faradaic current of the analyte, which forms a peak that defines the oxidation or reduction potential, the footprint of the analyte, depending on a direction of the potential program.

Voltammetric cell is used to conduct an experiment and contain two, or three electrodes connected to potentiostat as a source.

$$I = \frac{nFAc_{i0}\sqrt{D_i}}{\sqrt{\pi t}} \tag{2.9}$$

I – current, in A n – number of electrons (to reduce/oxidize one molecule of analyte i, for example) F = Faraday constant 96 485 $\mathrm{C\,mol^{-1}}$ A – area of the (planar) electrode in $\mathrm{cm^2}$ c_{j0} – initial concentration of the reducible analyte j in $\mathrm{mol\,cm^{-3}}$; D_j – diffusion coefficient for species i in $\mathrm{cm^2\,s^{-1}}$ t – time in s. $I = kt^{-1/2}$

Chapter 3

Experimental Part

3.1 Studied Analytes and Reagents

- TTF, TTF-BEDT, TTF-Der1, TTF-Der2, TTF-Der3[19]
- Ferrocene $C_{10}H_{10}Fe$
- Tetrabutylamonium hexafluorophosphate $TBAPF_6$ (electrochemical grade, Fluka)
- Chloroform $CHCl_3$
- Acetonitrile CH_3CN (anhydrous, 99.8 %, *Sigma-Aldrich*, Saint Louise, USA)
- 4–hydroxy–2,2,6,6–tetramethylpiperidin–1–oxyl (TEMPOL, 97 %, *Sigma-Aldrich*)

Following stock solutions were prepared:

- $0.25\,\mathrm{mol\,dm^{-3}}$ supporting electrolyte solution of $TBAPF_6$ in $CH_3CN : CHCl_3 = 1 : 1$;
- $8{\cdot}10^{-5}\,\mathrm{mol\,dm^{-3}}$ solution of samples in supporting electrolyte solution for quantitative EPR spectroscopy. All measured solutions were prepared in oven-dried vials, thoroughly purged with gaseous nitrogen, N_2 by weighing 1 mg of TTF-derivative on analytical scales, that was dissolved in a calculated volume of supporting electrolyte solution and subsequently purged for 2 minutes with N_2 to minimize the influence of atmospheric oxygen on the electrochemical experiments and on the EPR line broadening.
- other reference solutions were prepared in the concentration range from $1{\cdot}10^{-5}\,\mathrm{mol\,dm^{-3}}$ to $1{\cdot}10^{-4}\,\mathrm{mol\,dm^{-3}}$.

3.2 Instrumentation and Software

3.2.1 EPR Experimental

The EPR spectra were acquired by the Bruker EMX^{plus} 10/12 CW EPR spectrometer implemented with a microwave bridge, Premium-X-band. The g-factor of the radical cation was determined using an ER-036TM NMR-Teslameter and a built-in spectrometer frequency counter We used six methods for acquiring EPR spectra. Experimental parameters are stated in Table 3.1.

A flat EPR quartz cell (Bruker ER160FCQ) was used for room-temperature EPR spectroelectrochemical experiments.

A home-built three-electrode system consisting of a Pt wire with Pt μ-mesh (working electrode), an Ag wire (quasi-reference electrode), and a Pt-wire (counter electrode), inserted into the EPR cell and finally into the *Bruker* ER4102ST EPR cavity. For the radical cation, also the high sensitivity Bruker ER4119HS EPR cavity was used to obtain spectra with optimal resolution. Inactive electrode parts were isolated either with teflon tape or sealed in a glass capillary. The accuracy of the Ag quasi-reference electrode was corrected against the ferrocene/ferrocenium (Fc/Fc^+) couple. Simultaneous voltammetric and potentiostatic experiments were controlled by a Potentiostat (Galvanostat) Autolab PGSTAT302N (*Metrohm*). The experiments at lower (down to 248 K) temperatures were controlled by the Win-EPR acquisition software (both from *Bruker*) and a liquid/gas nitrogen unit ER 4141VT-U. During variable-temperature measurements, a compatible EPR flat cell (ER165FCVTQ, *Bruker*) with a 3-electrode system was used.

The g-factor, hyperfine splitting constant a, line width were deducted from the resulting spectra and microwave frequency, centre sweep, resolution and modulation amplitude were recorded. Following the calculation of hyperfine interaction constant A and determination of the number of equivalent nuclei. From all of these parameters simulations of the EPR spectra were performed with an EasySpin program (v. 5.1.10) in Matlab by least-squares fitting to an experimental spectrum using a combination of Nelder–Mead simplex and Particle swarm algorithms[48].

Table 3.1: Experimental parameters of methods for acquiring EPR spectra

type of examination	potentiostatic accumulation	simultaneous quantitative-EPR smaller cell	calibration of standards in double rectangular resonator	calibration of Mn standards	temperature measurements	stability of the radical cation
microwave frequency, GHz	9.795	9.812	9.812	9.853	9.527	9.796
microwave power, mW	5.024	2.52	2	2	3.99	3.99
receiver gain	10000	3999	1000	1000	10000	10000
modulation amplitude, mT	0.024	0.064	0.042	0.540	0.75	0.064
resolution, mT	0.005	0.098	0.03	0.009	0.01	0.008
Conversion time, ms	16	8	12	10	12	12
Time constant, ms	5.12	2.56	2.56	5.12	5.12	5.12

For EPR quantitative spectroscopy, intensities of individual spectra were recorded and compared to simulated spectrum to calculate the double integrals. The real number of radicals was determined by comparing the double integrals ($N_{\text{Samp.}} = (DI_{\text{Samp.}}/DI_{\text{Stand.}}) \cdot N_{\text{Stand.}}$) of the EPR spectra in the double-rectangular cavity versus the calibrated the commercially available EPR standard or determined by absolute mothod within the *Xenon* software for EPR spectrometer. The uncertainty was calculated from the several independent measurements ($DI_{\text{Samp.}}/DI_{\text{Stand.}}$) and by the theory of error propagation ($N_{\text{Samp.}}$) As shown in Section 3.3 Data analysis. These calculations were made with help of *R* and *Python* language scripts.

3.2.2 Voltammetry

Cyclic voltammograms were recorded on Potentiostat/Galvanostat Autolab PGSTAT302N (Metrohm).

The parameters of cyclic voltammetry (CV) were as follows: 15 s pretreatment at +0 mV, +0 mV start potential, +1000 mV final potential and 2.5 mV s^{-1} scan rate, if not mentioned differently. Data from voltammograms were saved as ".ocw" files that could be later used for processing and data analysis (*Python* language scripts). These include subtraction of capacitive current (baseline correction) and subsequent determination of Faradayic (peak) current, charge and evaluation of number of electrons from the Faraday law Equation (3.2) and correction of potentials according to ferrocene redox couple (determined from 8 independent measurements). Finally with combination of EPR, the ratio of the real number of radicals from EPR to the number of electrons, $N_{\text{Transferred-e}}$, was determined and correlated to the corresponding potentials E.

3.3 Data analysis

The data acquired and evaluated from EPR and Voltammetry experiments were inserted into various prepared Python and "R" scripts according to the need, that has processed and evaluated them into graphs or tables.

The process of data analysis for quantitative EPR spectroelectrochemisty was as follows: Voltammograms were acquired as I vs. E curve. The capacitive current was approximated by linear regression and subtracted. The data from I vs. E curve were then transferred to Q vs. E curve, through known scan rate and the Faraday law Equation (3.1) (peak current I vs time t). The real nmber of electrons was obained by

the Equation (3.2)(Avogadro constant N_A, Faraday constant F, valency number of ions). The data were then transferred from Q vs. E curve to $N_{\text{Transferred-e}}$ vs. E. Then from the simultaneous EPR spectroelectrochemisty experiments measured together with chosen EPR standard see Chapter 4,the number of generated radicals by comparing of double integrals of the manganese standard signal to the signal of studied cation radical was determined. In the next step the ratio of the real number of radicals from EPR to the number of electrons was determined and correlated to the corresponding potentials E. Finally the comprehensive graph was made for all experiments, individually for TTF and TTF–Der3, from which the confidence interval was determined by R programming language. The integration was done numerically within the R or Python scripts.

$$Q = \int_0^t I \, \mathrm{d}t \tag{3.1}$$

$$N_{\text{Transferred-e}} = \frac{N_A Q}{Fz} \tag{3.2}$$

3.3.1 Combination of t-Confidence Interval Determination and Error Propagation

In this section, there are shown the statistical methods, which are used to estimate the value of the physical property (the number of radical cations) and also to determine the confidence interval. The double integral (DI) ratio DI_{ratio} of simulated spectra of sample $DI_{\text{Samp.}}$ and our standard $DI_{\text{Stand.}}$ was used to evaluate the number of spins $N_{\text{Spin, Samp.}}$ from the number of unpaired electrons $N_{\text{Spin, Stand.}}$ in our simulations. These all are the key properties defined and described in the following equation

$$N_{\text{Spin, Samp.}} = \frac{DI_{\text{Samp.}}}{DI_{\text{Stand.}}} N_{\text{Spin, Stand.}} = DI_{\text{ratio}} N_{\text{Spin, Stand.}} \tag{3.3}$$

Confidence intervals of double integral in quantitative EPR

It is supposed that the measurements meet the assumptions of a normal distribution. For the finite number of measurements (we had 8 actually) we consequently obtain so-called *Student's t-distribution*, which took a name after a pseudonym of chemist William S. Gosset[51]. In this distribution, we can define the *confidence interval* that tells us the reliability of using single measurement DI_i as an estimator for the true value of

our whole. For N measurements the confidence interval can be written in the form

$$DI_{\text{ratio}} = \overline{DI_{\text{ratio}}} \pm t_{1-\alpha,\,N-1} \sqrt{\frac{\sum_{i=1}^{N} \left(DI_{i,\,\text{ratio}} - \overline{DI_{\text{ratio}}} \right)^2}{N\,(N-1)}} \tag{3.4}$$

where $\overline{DI_{\text{ratio}}}$ is an arithmetic mean value of N measurements of DI_{ratio}. In the coefficient of Student's distribution $t_{1-\alpha,\,N-1}$, variable α is the significance level and the expression $(1-\alpha)$ is the confidence level. In practice, the *standard deviation* σ is commonly used and defined in the following expression

$$\sqrt{\frac{\sum_{i=1}^{N} \left(DI_{i,\,\text{ratio}} - \overline{DI_{\text{ratio}}} \right)^2}{(N-1)}}. \tag{3.5}$$

Error Propagation

In our calculations of error propagation value, we have used the standard expression[51] for calculation of uncertainty u

$$u(N_{\text{Spin, Samp.}}) = \sqrt{\sum_{i=1}^{3} \left(\frac{\partial N_{\text{Spin, Samp.}}}{\partial x_i} \right)^2 u^2(x_i)} \tag{3.6}$$

on our formula for $N_{\text{Spin, Samp.}}$

Chapter 4

Results and Discussion

4.1 Voltammetric Studies

Cyclic voltammetry studies were performed in flat EPR cell for a series of TTF-Derivatives under current study and resulting voltammograms can be seen in Figure 4.1. As it was found and reported in the literature as well as shown by the EPR results, see Section 4.2, each compound undergoes two reversible redox steps from radical cation to dication. Half–wave potentials $E_{1/2}$, estimated from the peak potentials, can be found in Table 4.1. Apparently we can say that half–wave potentials rise from unsubstituted TTF derivative up to TTF–Der2, along with the molecular weight. The pattern is interrupted by TTF–Der3, whose has corresponding potential is smaller than that of TTF–Der2.

Table 4.1: Half–wave potentials of the first and the second redox step in $CHCl_3$:ACN; 1 : 1, 0.25 mol dm^{-3} $TBAPF_6$, at 5 mV s^{-1}, concentration 8·10^{-5} mol dm^{-3}

	$E_{1/2,1}$/V	$E_{1/2,2}$/V
TTF	-0.159	0.271
BEDT–TTF	0.057	0.362
TTF–Der1	0.17	0.44
TTF–Der2	0.176	0.498
TTF–Der3	0.143	0.431

Considering the fact that all studied substances were scanned under the same conditions, the pattern interruption of half–wave potential suggests the influence of a

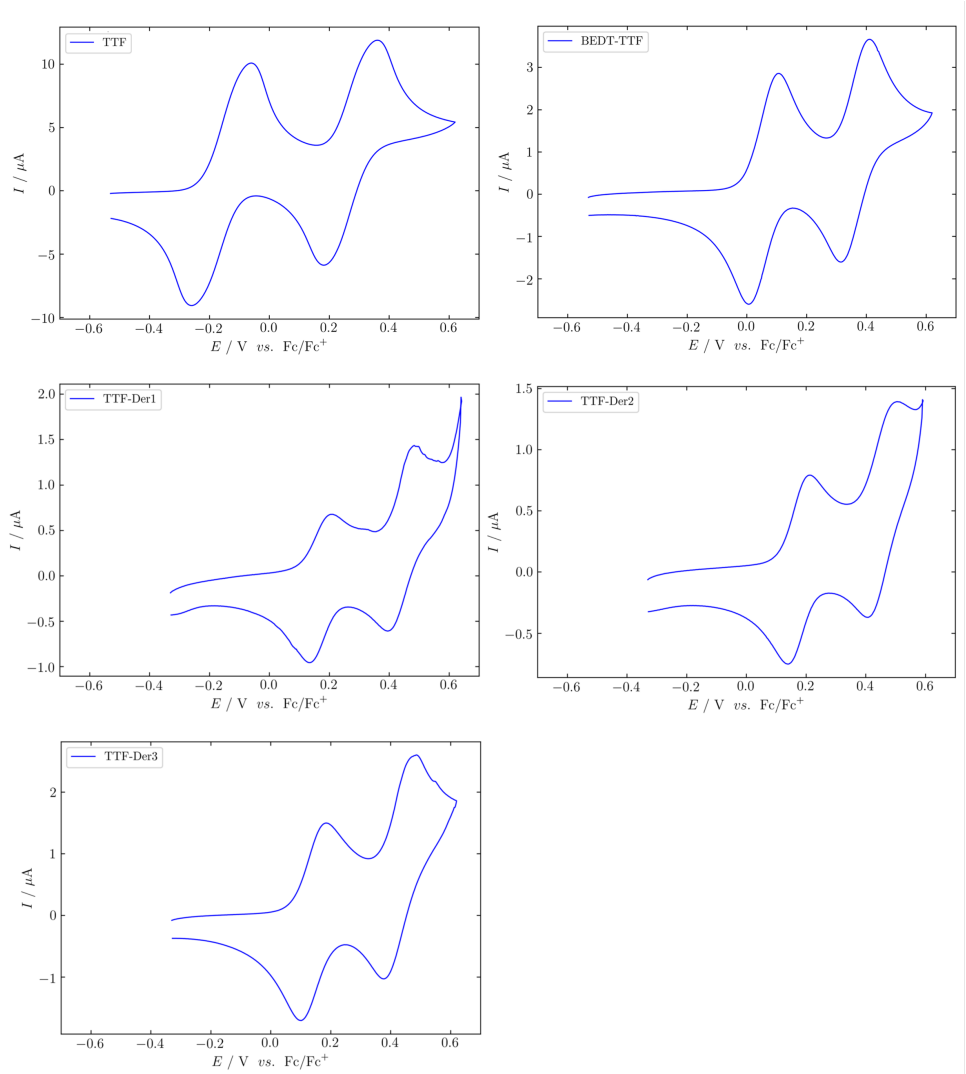

Figure 4.1: Cyclic voltammograms of TTF derivatives $8{\cdot}10^{-5}$ mol dm^{-3} in 1 : 1 ratio of $CHCl_3$: CH_3CN solvents at 5 mV s^{-1} scan rate

substituent on the redox properties. Substituted TTF derivative are more difficult to oxidize due to the pulling electron density away from the TTF unit. Because of the bonding through methylene, there is a possibility of rotating and structural conformation of the phenyl substituent against TTF and their interaction. It was deduced that the benzyl substituent gives the electron density back and that is why the half–wave potential is shifted to the left.

To check the stability of quasi–reference silver electrode, we used ferrocene/ferrocenium redox couple's half–wave potential as a reference, because two different cells and two different electrode systems were used. The value for bigger cell for voltammetric

and EPR characterisation reads (0.33 ± 0.01) V and the value for the small one reads (0.499 ± 0.005) V, the uncertainty was calculated from five independent measurements.

4.1.1 Potential Scan Rate Dependence

Cyclic voltammograms of TTF–Der3 acquired at different scan rates from 2.5 mV s^{-1} to 80 mV s^{-1} by three consecutive scans. The dependence of peak current to the scan rate and its square root can be seen in the Figure 4.2. Apparently the peak current is directly proportional to the square root of scan rate that suggests that the process of oxidation is diffusion controlled and therefore the probability for adsorption, taking place, is minimal. The slope and intercept of the first oxidation step are 0.51 ± 0.01 and 0.17 ± 0.05 respectively, with 0.999 value of coefficient of determination. The slope and intercept of the second oxidation step are 0.75 ± 0.01 and 0.24 ± 0.07 respectively, with 0.998 value of coefficient of determination.

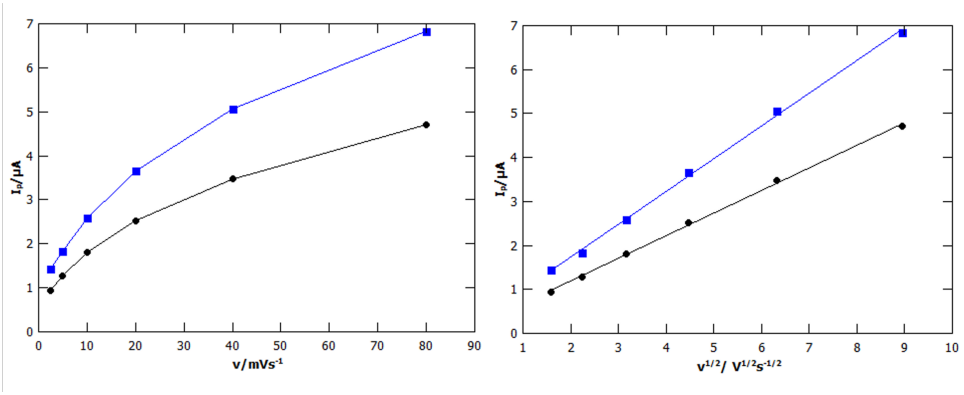

Figure 4.2: Dependence of peak current I_p of the first (lower, black dotted line) and the second (upper, blue squared line) oxidation step of $8{\cdot}10^{-5}$ mol dm^{-3} TTF–Der3 on scan rate (left) and the square root of scan rate (right) in 1 : 1 ratio of $CHCl_3$: CH_3CN solvents at potential scan rate of 2.5 mV s^{-1} to 80 mV s^{-1}.

4.2 Basic EPR Spectroelectrochemical Studies

In the EPR/ESR studies, the unpaired electron (spin) density information was investigated. Because different TTF–derivatives were probed, it was important to show that the oxidation runs at the TTF unit and not at the substituents. This was achieved by the combination of EPR and CV. These studies lead to following results, Figure 4.3, in the form of representative spectra for each derivative and the dependence of the

intensity of double integral of EPR signal to the individual potentials against Fc/Fc^+ redox couple.

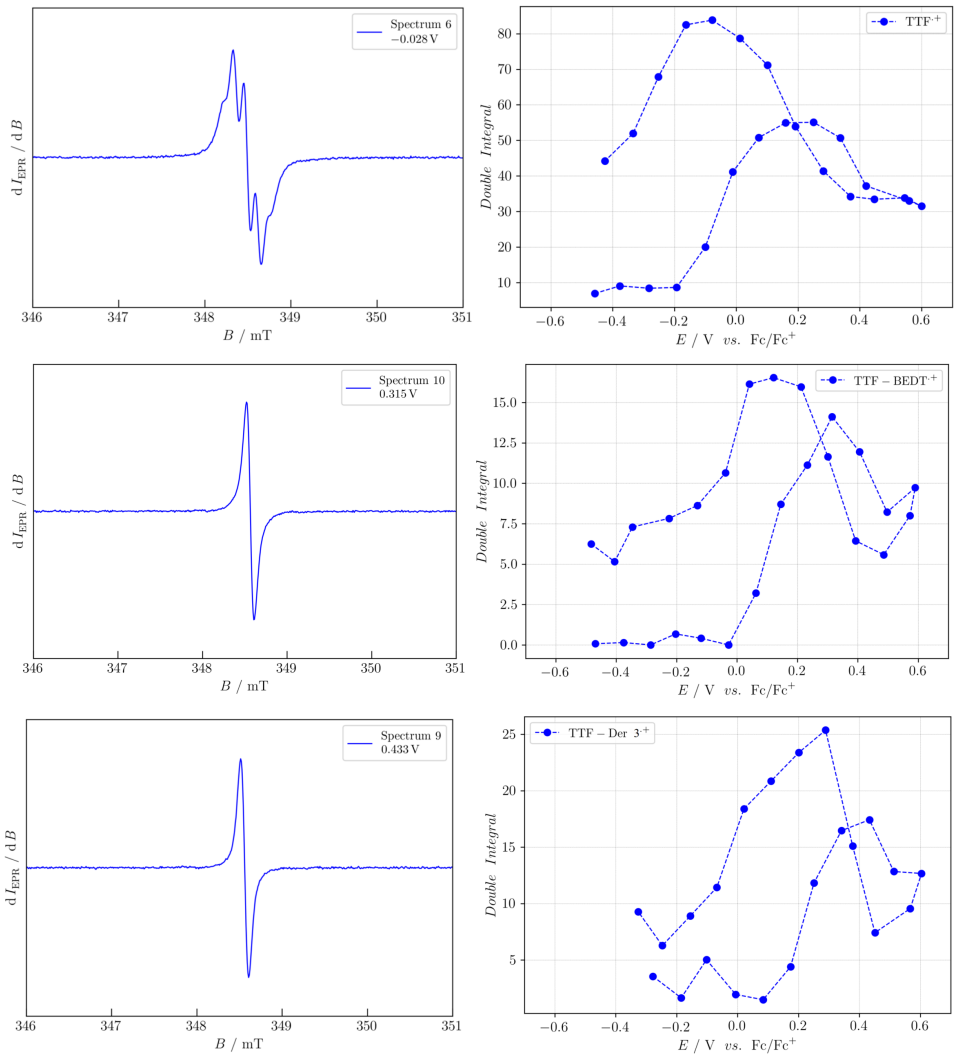

Figure 4.3: Representative EPR spectra (left) of TTF–DerX$^{\bullet+}$, BEDT–TTF$^{\bullet+}$ and TTF-Der3$^{\bullet+}$ with corresponding dependencies (right) of double integral to oxidation potential, where the spectra were acquired with $8{\cdot}10^{-5}$ mol dm^{-3} solution in 1 : 1 ratio of $CHCl_3$: CH_3CN at 5 mV s^{-1} scan rate.

Parameters of EPR spectra can be found in Table 4.2. They were obtained from simulations of EPR spectra. It was found that these match the experimental ones. The EPR spectrum of TTF shows a "broader" quintet (pentet), a hyperfine splitting, which is due to the four equivalent ^{1}H nuclei in the vicinity of the unpaired electron. The natural abundance of ^{1}H is 99.99 %, in comparison with the ^{33}S and corresponding abundance of 0.75 % as well as ^{13}C abundance of 1.07 % could not be distinguished

Table 4.2: Parameters (g-factor and A, hyperfine coupling constants) obtained from simulated EPR spectra.

	A/MHz of equivalent nuclei	g–factor
$TTF^{\bullet+}$	$4 \times (^{1}H) = 3.522$	2.0081
$BEDT^{\bullet+}$	$2 \times (^{13}C) = 3.026$ $4 \times (^{33}S) = 9.771$ $4 \times (^{13}C) = 1.829$ $4 \times (^{33}S) = 0.700$	2.0079
TTF–$Der3^{\bullet+}$	$2 \times (^{13}C) = 4.752$ $4 \times (^{33}S) = 10.004$ $4 \times (^{13}C) = 2.701$ $4 \times (^{33}S) = 0.818$	2.0079

due to the broader signal. On the other hand, all the other derivatives have the proton positions substituted and therefore just one line is observed because of small natural abundance of magnetically active nuclei, which appear as small satellites.

These observations corroborate that the electron transfer takes place at the TTF–unit and not at the substituent-site. Therefore, the spin density is also highest at the TTF–unit of the $TTF^{\bullet+}$. Subsequently, the simulated EPR spectra were used for the quantitative EPR analysis, because of low signal-to-noise ratio and therefore the double integrals were evaluated from the corresponding simulated spectra.

In the right side of Figure 4.3 occurrence of comproportionation reactions are observed. We can divide each graph into four steps in the forward direction of a scan, these are the capacitive current region, where no "Faradayic" reaction takes place and can be evaluated by linear regression with a straight line, then the first oxidation to cation radical (e.g. $TTF-BEDT \rightleftharpoons TTF-BEDT^{\bullet+} + e^{-}$), here the rising tendency of double integral is observed, than the second oxidation to dication (e.g.:$TTF-BEDT^{\bullet+} \rightleftharpoons TTF-BEDT^{2+} + e^{-}$), where the signal falls down due to diamagnetism and finally comproportionation of dication with neutral molecule to form radical cation again leads to slight increase of the signal. These regions are summarized in the Table 4.3.

sectionQuantitative Simultaneous EPR Voltammetric Studies

Table 4.3: Characteristic Potential Regions (E *vs* Fc/Fc^+) for the Generation of Radical Cations.

TTF–Derivative	no reaction	radical cation gener.	gener. of dications	comproporionation
TTF	−0.5 V to 0.2 V	−0.2 V to 0.2 V	0.2 V to 0.6 V	–
TTF–BEDT	−0.5 V to 0.0 V	0.0 V to 0.3 V	0.3 V to 0.5 V	0.5 V to 0.6 V
TTF–Der3	0.3 V to 0.1 V	0.1 V to 0.4 V	0.4 V to 0.6 V	–

4.2.1 Standards for Quantitative EPR

Following commercially available EPR standards (for quantitative analysis) were available:

- Mn^{2+} in ZnS (*Magnettech*[52])
- Cr^{3+} in MgO (*Magnettech*[52])
- "Strong Pitch" (*Bruker*, supplied with EPR spectrometer)

Except the "Srong Pitch",which possess a single-line without a hyperfine splitting, the EPR spectra of the two standards, supplied by company *Magnettech GmbH* (Germany), are depicted in Figure 4.4.

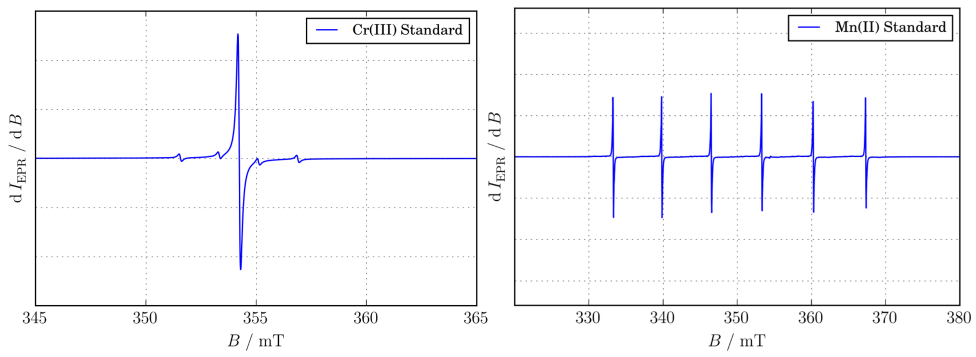

Figure 4.4: EPR scan of Chromium standard (left) and Manganese standard (right) at 293 K, centered at $g = 1.9800$ and 2.0024, respectively.

In the case of chromium and low concentration of our analytes, $1{\cdot}10^{-5}$ mol dm^{-3} to $1{\cdot}10^{-4}$ mol dm^{-3}, complicated baseline corrections are required and also overlap of spectral characteristics (lines) of our analytes occurs. For the same reason of overlapping the Strong Pitch sample was also not suitable for simultaneous comparison of double integrals. It was found that Manganese standard was more suitable for the location and

integration of the spectrum, because the majority of organic radicals (including the TTF–Derivatives) exhibit EPR spectra between third ($g = 2.0267$) and fourth ($g = 1.9858$) line of manganese spectrum (see also).

Mn^{2+} in ZnS had to be calibrated and the number of paramagnetic centers corresponding to third and fourth line was found out. The real number of radicals was determined by comparing the double integrals (DI) ($N_{\text{Samp.}} = (DI_{\text{Samp.}}/DI_{\text{Stand.}}) \cdot N_{\text{Stand.}}$) of the EPR spectra in the double-rectangular cavity versus the Strong-Pitch Bruker reference by several independent experiments and determined (including the uncertainty) by combination of confidence interval determination ($DI_{\text{Samp.}}/DI_{\text{Stand.}}$) and error propagation ($N_{\text{Samp.}}$), see also Section 3.3. By the *Bruker-Xenon* software and several measurements within the high sensitivity EPR cavity, it was found out that the double integral of the Strong Pitch reads $(2.05\pm0.05)\cdot10^{16}$ paramagnetic species, which corresponds $(5.1\pm0.2)\cdot10^{15}$ per effective cm tube length.

By the above-described calibration experiments following number of paramagnetic species, corresponding to 3rd and 4th Mn^{2+} EPR spectral lines were determined: $(4.2\pm0.3)\cdot10^{15}$ and $(4.1\pm0.2)\cdot10^{15}$, respectively. It means we can use any of these lines, as far as it corresponds to almost the same value as well as the uncertainty.

The experimental layout for quantitative EPR spectroelectrochemistry is shown in Figure 4.5. This experimental layout and its corresponding quantitative determination of paramagnetic particles were validated with TEMPOL-sample with known concentration ($1\cdot10^{-4}\,\text{mol}\,\text{dm}^{-3}$, corresponding to $(1.29\pm0.01)\cdot10^{15}$ number of $\text{TEMPOL}^{\bullet+}$ species). The comparison of the spectral double integrals of the third and the fourth line to the spectral double integral of TEMPOL corroborated the calculated values against Strong Pitch reference and finally the number of TEMPOL-radicals $(1.3\pm0.1)\cdot10^{15}$ was determined. Hence the experimental setup with manganese standard was validated.

4.2.2 Reproducible Quantitative EPR Voltammetric Experiments

The data obtained from EPR spectroelectrochemichal experiments were processed and analyzed by above mentioned procedure and can be seen in Chapter 3.The spectra were acquired in 3–4 consecutive experiments and then fresh new solution with clean electrodes was conducted also 3- to 4-times. So each quantitative EPR spectroelectrochemical experiment was measured at least six times.

First of all the dependence of the ratio of the generated radicals to the transferred electrons $N_{\text{Radicals}}/N_{\text{Transferred-e}}$ on the potentials were depicted in the graphs Figure 4.6 of TTF at different scan rates, in order to obtain more general dependency. It was

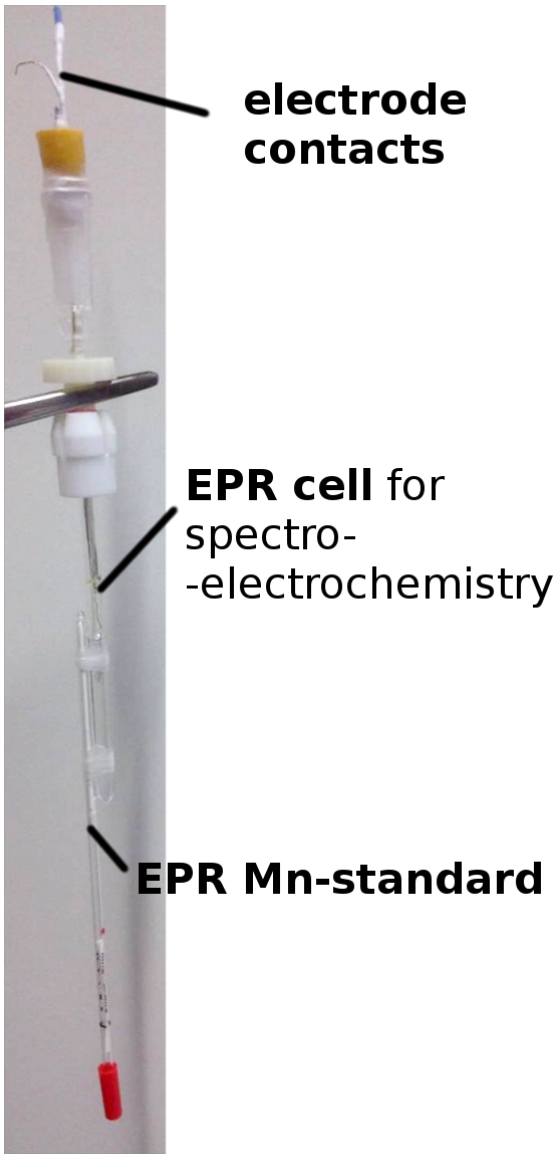

Figure 4.5: Experimental layout with reference and three electrode system

observed that the rate of $10\,\mathrm{mV\,s^{-1}}$ was not very convenient for this experimental layout and quantitative analysis, because we cannot determine the maximum very well and the number of points was rather low.

Secondly all of the data from Figure 4.6 were together implemented into the second comprehensive graph Figure 4.7 and the 95 % confidence interval was determined, as can be seen in the Figure 4.7. For this purpose the method from *statistical programming language R (ggplot2)* was applied. The method in *ggplot2* works as a "t–based" approximation of local regression method, with "span" parameter, which is a fraction of a

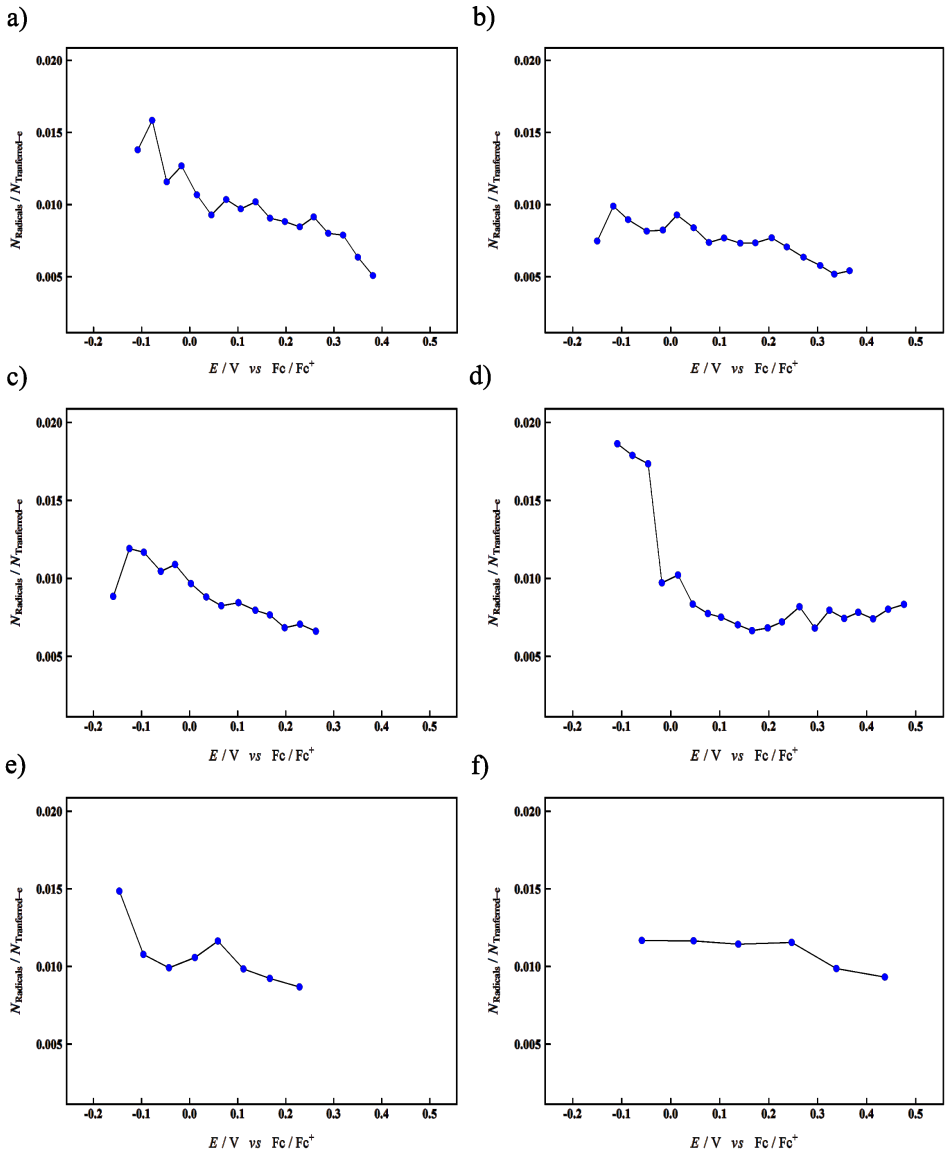

Figure 4.6: The dependence of the ratio of the generated radicals to the transferred electrons $N_{\text{Radicals}} / N_{\text{Transferred-e}}$ on the potentials from representative samples of $8{\cdot}10^{-5}$ mol dm^{-3} TTF, a)–d) 2.5 mV/s, e) 5 mV/s and f) at 10 mV/s

points to fit each local regression and the value 0.32 span was used. The data were also modeled by linear regression using the polynomial function of the $6-th$ and $7-th$ order and the same results like with t–based approximation was found.

This method was also applied in the same way to TTF–Der3$^{\bullet+}$ for whole forward linear sweep electrochemical oxidation (reverse sweep was not considered for the clarity). Graphically determined confidence inerval (grey area) for the dependences of the ratio of the generated radicals to the transferred electrons on the potentials for

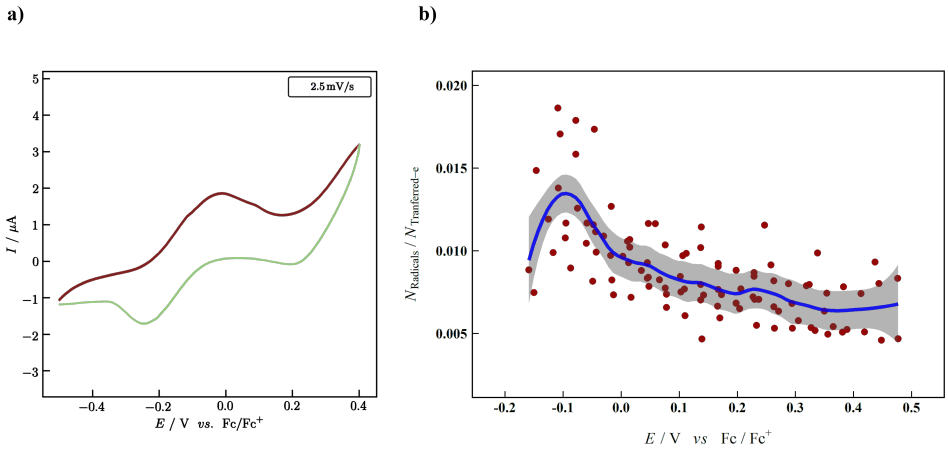

Figure 4.7: a) Comprehensive graph of the dependence of the ratio of the generated radicals to the transferred electrons $N_{\text{Radicals}}/N_{\text{Transferred-e}}$ on the potentials for TTF$^{\bullet+}$ with the obtained confidence interval (gray region). b) In cyclic voltammogram the forward linear scan is highlighted, from which the number of transferred electrons was estimated.

both TTF$^{\bullet+}$ and TTF–Der3$^{\bullet+}$ is $\pm$0.001 and therefore the method of confidence interval determination is not dependent on the studied compound. As can be seen from both Figure 4.7 and Figure 4.8 the potential, at wich maxima are observed matches the potential region, corresponding to the first oxidation step.

The local maximum for TTF–Der3$^{\bullet+}$ in the region of 0 V vs Fc/Fc^{+} is caused by an error in determination of number of radicals, when due to the repeated expriments a small number of radicals remained at the beginning of the process.

The differrence of maximal ratios for TTF$^{\bullet+}$ is 0.014$\pm$0.001 and TTF–Der3$^{\bullet+}$ is 0.011$\pm$0.001. The ratio of generated radicals to transferred electrons in the case of TTF$^{\bullet+}$ 0.003 greater than in case of TTF–Der3$^{\bullet+}$, which suggests that TTF–Der3$^{\bullet+}$ has higher tendency to form diamagnetic associates than standard TTF$^{\bullet+}$. Despite of quasi–reversible voltammetric characteristics, the presence of follow–up reactions was proven like it was already reported for very similar thiophene compound[53].

Even though the determination of the dependence of the ratio of the generated radicals to the transferred electrons on the potential indicates higher tendency to form associates in the case of TTF–Der3$^{\bullet+}$, due to the presence of aliphatic chains, in future studies the concentration dependencies and the dependency on solvent will be taken into

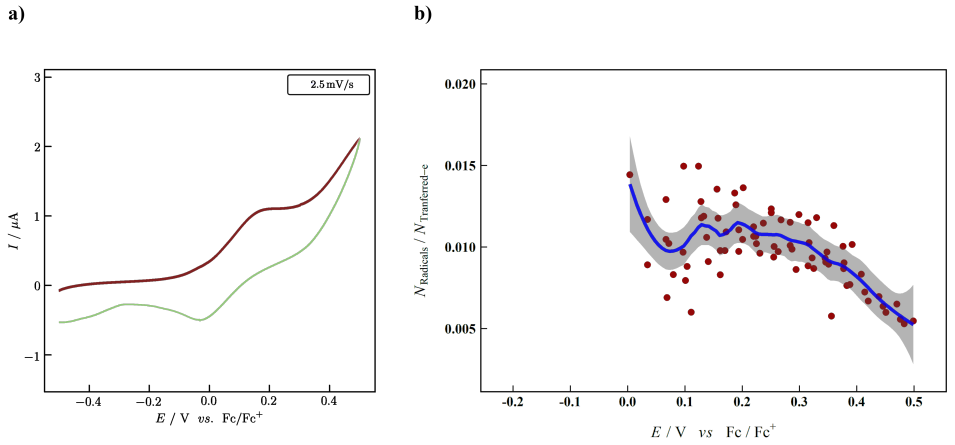

Figure 4.8: a) Comprehensive graph of the dependence of the ratio of the generated radicals to the transferred electrons on the potential for TTF–Der3$^{\bullet+}$ with the obtained confidence interval (gray region). b) In cyclic voltammogram the forward linear scan is highlighted, from which the number of transferred electrons was estimated.

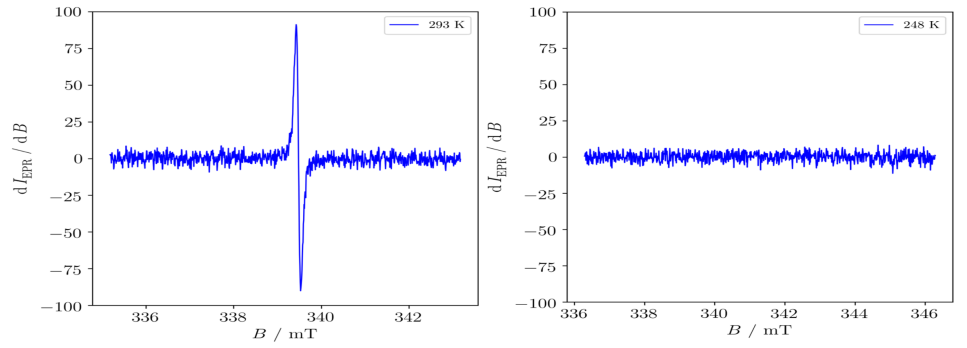

Figure 4.9: Temperature dependent EPR measurement of $8{\cdot}10^{-5}$ mol dm^{-3}TTF-Der3, left 293 K, right 248 K

consideration, as well. Additionally, TTF with other electron-withdrawing/donating substituents should be check in order to complete the more general picture.

The dimerization/association of radical cations was additionally supported by temperature dependent EPR experiments, because by lowering the temperature the equilibrium of the process is shifted towards diamagnetic dimers/association, which are not seen by EPR (see Figure 4.9).

Chapter 5

Summary

TTF substituents affect the charge transfer (CT) complex of the tetrathiafulvalene radical cation and the tetracyanoquinodimethane radical anion. This was visible from EPR spectra. We investigated five compounds and determined EPR parameters (g-factor, A-hyperfine coupling constant) of TTF, BEDT–TTF and TTF–Der3. The parameters for TTF-Der2 and TTF-Der1 and BEDT–TTF were very similar due to their structural resemblance. Next, the ratio of the transferred charge to the number of generated radicals was determined for representative TTF and TTF–Der3 by quantitative EPR spectroelectrochemistry. The presence of subsequent reactions (e.g. dimerization)after the electron transfer was also detected by a combination of EPR and CV. Oxidation takes place on the TTF moiety of the molecule for all five studied derivatives, which was claimed by the EPR spectroscopy and hyperfine splitting, which also means higher spin density on this part of the molecule. It was found that the half-wave potentials of the individual TTF derivatives increase in a sequence from the unsubstituted TTF to the TTF–Der2 the "methylenecyclohexyl" derivative (in the first oxidation step from -0.159 V to 0.176 V and in the second oxidation step from 0.271 V to 0.498 V) and the decline in half-wave potentials (both ox. steps) is observed in the TTF–Der3 "benzyl" derivative(the first oxidation step from 0.143 V and the second oxidation step from 0.431 V). The dependence of the peak current on the square root of the scan rate claimed the diffusion process. EPR and voltammetric analysis pointed to the intramolecular interaction of TTF–moiety and benzyl group within TTF–Der3. However, in order to confirm the intramolecular interaction, the study will be done with additional donor/acceptor substituent.

For quantitative EPR spectroelectrochemical analysis studies of radical cations, the most suitable standard was selected, it is Mn^{2+} in ZnS, although further consultation

with the producer about the reduction of paramagnetic centres and the manganese standard concentration would be suitable to match lower sample concentrations. The ratio of the electrochemically generated radical cations to the number of electrons transferred (identified from voltammetry curves and Faraday Law) for $TTF-Der_3^{\bullet+}$ is 5.5 : 500 and for $TTF-Der_3^{\bullet+}$ is 7 : 500. The ratio shows that the $TTF-Der_3^{\bullet+}$ is more prone to perform presence subsequent chemical reactions (e.g. dimerization/association) because it is substituted with longer aliphatic chains. It was determined by several independent measurements for the derivatives : TTF, TTF–Der3.

Appendices

Appendix A

List of Abbreviations

BEDT–TTF	Bis(ethylenedithio)–TTF
CT	Charge Transfer
CV	Cyclic voltammetry
DME	Dropping Mercury Electrode
EPR	Electron Paramagnetic Resonance
ESR	Electron Spin Resonance
IET	Intramolecular Electron Transfer
L–B	Langmiur–Blodgett
NMR	Nuclear Magnetic Resonance
OFET	Organic Field–Effect Transistor

SCE	Saturated Calomel Electrode
SOMO	Single Occupied Molecular Orbital
TCNQ	Tetracyanoquinodimethane
TEMPOL	4–hydroxy–2,2,6,6–tetramethylpiperidin–1–oxyl
TTF	Tetrathiafulvalene

Appendix B

Physical Quantities and Units

a	hyperfine splitting constant	G (mT)
A	hyperfine interaction constant – A/h	MHz (cm^{-1})
N_A	Avogadro constant	$6.022\,140\,86 \cdot 10^{23}\,mol^{-1}$
c	concentration	$mol\,dm^{-3}$
I	current	A
I_p	peak current	A
e	elementary charge	$1.602\,177 \cdot 10^{-19}\,C$
E	potential	V
F	Faraday constant	$96\,485\,C\,mol^{-1}$
g_e	g–factor (dimensionless)	2.002 319
g_p	g–factor (dimensionless)	5.585 694
h	Planck's constant	$6.626\,070 \cdot 10^{-34}\,J\,s$
$\hbar$	dirac constant	$1.054\,572 \cdot 10^{-34}\,J\,s\,rad^{-1}$

$\vec{L}$	orbital angular momentum	N m s ($\mathrm{kg\,m^2\,s^{-1}}$)
$\vec{B}_0$	magnetic flux density	T ($\mathrm{kg\,s^{-2}\,A^{-1}}$)
γ_e	magnetogyric ratio of an electron	$\mathrm{Ckg^{-1}}$ ($\mathrm{rads^{-1}T^{-1}}$
m_e	mass of the electron	$9.109\,384{\cdot}10^{-31}$ kg
m_p	mass othe proton	$1.672\,622{\cdot}10^{-27}$ kg
$\vec{\mu}$	magnetic dipole moment	$\mathrm{J\,T^{-1}}$ ($\mathrm{A\,m^2}$)
μ_B	bohr magneton	$9.27{\cdot}10^{-24}\,\mathrm{J\,T^{-1}}$ ($\mathrm{A\,m^2}$)
Q	charge	C (A s)
$\vec{S}$	spin angular momentum	N m s ($\mathrm{kg\,m^2\,s^{-1}}$)
t	time	s

Appendix C

Code Examples for Data Analysis

All scripts were written by supervisor of the master thesis.

```r
library(readxl)
library(ggplot2)
library(extrafont)
loadfonts(device = "win")

# Loading data(table) with N_radical/N_electron ratio vs E / V (Fc/Fc+)
# summarized from all experiments:
entire.out.data <- file.path("Summ_Quant_Tables","All_TTF_Mn_quant_ratios_B.xlsx")
entire.out.table <- read_excel(entire.out.data,sheet = "Sheet1")

# Plot theme:
my.theme <- theme_bw() + theme(panel.grid = element_blank(),
axis.title = element_text(color = "black",size = 14,family = "serif"),
axis.text.x = element_text(face = "bold", color = "black", size = 12,
    family = "serif", margin = margin(10,10,10,10,unit = "pt")),
axis.text.y = element_text(face = "bold", color = "black", size = 12,
    family = "serif", margin = margin(10,10,10,10,unit = "pt")),
panel.border = element_rect(color = "black",size = 1.0),
axis.ticks.length = unit(-6,"pt"), plot.margin = margin(16,16,16,16,unit = "pt"))

# Elementary scatter plot including the linear regression model
# by the polynomial 6th-order curve and 95% confidence interval (by default):
base.ent.plot <- ggplot(data = entire.out.table,aes(x=E_V_vs_Fc,y=N_Ratio))
+ geom_point(color="brown",size=2.4)
+ geom_smooth(method = "lm", formula = y ~ poly(x, 6),color=alpha("blue",0.64),size=1.5)

# Axis title, labeling and ranges:
base.ent.plot + labs(x = expression(paste(italic(E)," / V   ", italic(vs), "   Fc / Fc"^{"+"})),y =
    expression(paste(italic(N)[Radicals]," / ",italic(N)[Tranferred-e])))
+ scale_x_continuous(limits = c(-0.22,0.52), breaks = c(-0.2,-0.1,0.0,0.1,0.2,0.3,0.4,0.5))
+ scale_y_continuous(limits = c(0.002,0.02)) + my.theme

# Saving the resulting figure with parameters:
ggsave("Summ_Quant_Figures/All_TTF_Mn_quant_ratios_B.png", width = 7, height = 5, units = "in",
 dpi = 400, bg = "transparent")
```

Figure C.1: Script written in R statistical language to create a scatter plot radicals-to-transferred electron ratios vs potential from all data obtained by quantitative EPR spectroelectrochemical experiments. Determination of 95% confidence interval by linear regression with 6th-order polynomial function.

```
# Capacitive current approximated by straight line (by linear regression model):

want_i_corr = input('CORRECTION FOR CAPACITIVE CURRENT ?, yes/no ').lower()

lin_constants = input('ENTER the "B"-intercept and "A"-slope,'+'\n'+
                      'respectively, for capacitive I, and separated by " ":  ').split()
lin_const_B,lin_const_A = map(float,lin_constants)

cv_df['Current / A'] -= (lin_const_B + cv_df['Potential / V']*lin_const_A)

# ------------------------------------------------------------------------------------

# --------------- Potential scale and its calibration -----------------
# ----vs. half-wave potential of the Fc/Fc^+ redocx couple ------

potential_Fc = float(input('ENTER the ESTIMATED HALF-WAVE POTENTIAL for the Fc/Fc^+ COUPLE:  '))

cv_df['Potential / V'] -= potential_Fc

# ------------------------------------------------------------------------------------

cv_df = cv_df[['Point','Potential / V','Current / A']]
cv_df.head()

# ------------------------------------------------------------------------------------

# -------- Scan rate data arrays and calculating charge/number of electrons -------------

scan_rate = float(input('ENTER the SCAN RATE in mV/s:  '))
scan_rate *= 1e-3                  # to convert mV/s to V/s

E_max = cv_df.loc[cv_df['Potential / V'].idxmax()][1]
E_min = cv_df.loc[cv_df['Potential / V'].idxmin()][1]

cv_df['time / s'] = (cv_df['Point']-1)*(2*(E_max-E_min)/(scan_rate*(len(cv_df['Potential / V'])-1)))

cv_df = cv_df[['Point','time / s','Potential / V','Current / A']]

data_cv = cv_df.as_matrix()

t = np.array(data_cv[:,1])          # t => time in seconds
E = np.array(data_cv[:,2])          # E => Potential in Volts
I = np.array(data_cv[:,3])          # I => Current in Amperes

# Intedgration of I vs t to obtain charge-array and number of electrons:

N_A = const.value('Avogadro constant')
F = const.value('Faraday constant')

Q = integ.cumtrapz(I, t, initial=0)  # Q => Charge in Couloumbs

cv_df['Charge / mC'] = Q*1e+3        # Charge in mC

cv_df['Number of e-'] = Q*N_A/F      # Number of electrons

cv_df['Current / A'] *= 1e+6         # Convert current into micro Amps

# current in micro Amps (rename column):
cv_df.rename(columns={'Current / A':'Current / micro A'}, inplace=True)

# ------------------------------------------------------------------------------------
```

Figure C.2: Python script to calculate the charge and number of transferred electrons by the integration of the original cyclovoltammetric curve measured by *Autolab* potentiostat. Additionally the data can be exported as various table formats.

```r
library(readxl)

# Loading the data table including potential, double integrals
# and number of electrons (as columns):
q.data <- file.path("..","EPR","Tables_EPR","All_TTF_Mn_quant_a.xlsx")

q.data.table <- read_excel(q.data,sheet="Sheet1")

potential.Fc.V <- 0.499 # Estimated E1/2 of Fc/Fc+ couple in Volts (from CV)

N.Mn03 <- 4.17e+15 # Number of paramag. centers corresponding to 3rd Mn2+ EPR line

# Column corresponding to potential against Fc/Fc+ redox couple:

potential.V <- q.data.table$E_V - potential.Fc.V

q.data.table$E_V_vs_Fc <- potential.V

# Subtracting the double integral from 'non-faradayic'/'capacitive' region:
q.data.table$DI_TTFradCat <- q.data.table$DI_TTFradCat - min(q.data.table$DI_TTFradCat)

# Number of TTF radicals (radical cations):
N.TTFRad <- (q.data.table$DI_TTFradCat/q.data.table$DI_Mn03)*N.Mn03

# New column corresponding to number of radicals:
q.data.table$N_TTFradCat <- N.TTFRad

q.data.table <- q.data.table[c(5,1,2,3,6,4)] # reordering columns in dataframe

q.data.table$E_V <- NULL # deleting the column with original potential values

# Calculating the number of radicals-to-trans.e.-ratio:
N.TTFRad.e.Ratio <- q.data.table$N_TTFradCat/q.data.table$N_e

# New column corresponding to above-described ratio:
q.data.table$N_Ratio <- N.TTFRad.e.Ratio

# Removing meaningless values (corresponding to ratio < 0):
q.data.table <- subset(q.data.table,N_Ratio > 0)

head(q.data.table) # Showing the head of the table

#save the final data.frame/table:
write.table(q.data.table,"Summ_Quant_Tables/All_TTF_Mn_quant_a.csv",sep = ",",row.names = F)
```

Figure C.3: Script written in R statistical language to calculate the ratio of radicals-to-transferred electrons from comparison of double integrals of standard and those of sample. Data can be exported to ".csv" table format.

Bibliography

[1] J. Ferraris, D. O. Cowan, V. Walatka, J. H. Perlstein, *Journal of the American Chemical Society* **1973**, *95*, 948–949.

[2] J. J. Mayerle, J. B. Torrance, J. I. Crowley, *d. Chem. Soc. Perkin Trans* **1979**, *9*, 2995–2999.

[3] A. Girlando, R. Bozio, C. Pecile, J. B. Torrance, *Phys. Rev. B* **1982**, *26*, 2306–2309.

[4] M. Lamache, H. Menet, A. Moradpour, *Journal of the American Chemical Society* **1982**, *104*, 4520–4524.

[5] B. T. Zhao, M. J. Blesa, F. Le Derf, D. Canevet, C. Benhaoua, M. Mazari, M. Allain, M. Sallé, *Tetrahedron* **2007**, *63*, 10768–10777.

[6] M. Riordan, *Reviews of Modern Physics* **1999**, *71*, 7–28.

[7] S. Venneri, J. Wilson, J. M. Rawson, M. Pilkington, *ChemPlusChem* **2015**, *80*, 1624–1633.

[8] H. L. Van De Wouw, J. Chamorro, M. Quintero, R. S. Klausen, *Journal of Chemical Education* **2015**, *92*, 2134–2139.

[9] A. Coskun, J. M. Spruell, G. Barin, A. C. Fahrenbach, R. S. Forgan, M. T. Colvin, R. Carmieli, D. Benitez, E. Tkatchouk, D. C. Friedman, A. A. Sarjeant, M. R. Wasielewski, W. A. Goddard, J. F. Stoddart, *Journal of the American Chemical Society* **2011**, *133*, 4538–4547.

[10] J. Jalkh, Y. R. Leroux, A. Vacher, D. Lorcy, P. Hapiot, C. Lagrost, *The Journal of Physical Chemistry C* **2016**, acs.jpcc.6b09459.

[11] R. Mulliken, W. B. Person, *Annu. Rev. Phys. Chem* **1962**, *13*, 107–126.

[12] K. Walzer, B. Maennig, M. Pfeiffer, K. Leo, **2007**, 1233–1271.

[13] G. Sini, J. S. Sears, J. L. Brédas, *Journal of Chemical Theory and Computation* **2011**, *7*, 602–609.

[14] R. Pauliukaite, A. Malinauskas, G. Zhylyak, U. E. Spichiger-Keller, *Electroanalysis* **2007**, *19*, 2491–2498.

[15] J. Kulys, V. Simkeviciene, I. J. Higgins, *Biosens. Bioelectron.* **1992**, *7*, 495–501.

[16] M. R. Bryce, *J. Mater. Chem.* **2000**, *10*, 589–598.

[17] J. L. Segura, N. Martn, *Angew. Chemie - Int. Ed.* **2001**, *40*, 1372–1409.

[18] X. Gao, W. Qiu, Y. Liu, G. Yu, D. Zhu, *Pure and Applied Chemistry* **2008**, *80*, 2405–2423.

[19] B. J. Holec, MA thesis, **2012**.

[20] Y. Takahashi, J. Hasegawa, Y. Abe, Y. Tokura, K. Nishimura, G. Saito, *Appl. Phys. Lett.* **2005**, *86*, 1–3.

[21] T. Hasegawa, K. Mattenberger, J. Takeya, B. Batlogg, *Phys. Rev. B - Condens. Matter Mater. Phys.* **2004**, *69*, 3–8.

[22] J. P. Bourgoin, M. Vandevyver, A. Barraud, G. Tremblay, P. Hesto, *Mol. Eng.* **1993**, *2*, 309–314.

[23] N. Akhtar in *PhD Thesis*, **2013**.

[24] V. Morisson, C. Mingotaud, B. Agricole, M. Sallé, A. Gorgues, C. Garrigou-Lagrange, P. Delhaès, *J. Mater. Chem.* **1995**, *5*, 1617–1624.

[25] T. C. Narayan, T. Miyakai, S. Seki, M. Dinca, *Journal of the American Chemical Society* **2012**, *134*, 12932.

[26] D. R. Talham, *Chemical Reviews* **2004**, *104*, 5479–5501.

[27] J. M. Spruell, *Pure and Applied Chemistry* **2010**, *82*, 2281–2294.

[28] C. Wang, S. M. Dyar, D. Cao, A. C. Fahrenbach, N. Horwitz, M. T. Colvin, R. Carmieli, C. L. Stern, S. K. Dey, M. R. Wasielewski, J. F. Stoddart, *Journal of the American Chemical Society* **2012**, *134*, 19136–19145.

[29] I. Aprahamian, J. C. Olsen, A. Trabolsi, J. F. Stoddart, *Chemistry - A European Journal* **2008**, *14*, 3889–3895.

[30] L. Chen, Y. C. Zhang, W. K. Wang, J. Tian, L. Zhang, H. Wang, D. W. Zhang, Z. T. Li, **2015**, *26*, 811–816.

[31] A. Y. Ziganshina, Y. H. Ko, W. S. Jeon, K. Kim, *Chem. Commun.* **2004**, 806–807.

[32] C. A. Christensen, L. M. Goldenberg, M. R. Bryce, J. Becher, *Chem. Commun.* **1998**, 509–510.

[33] H. Spanggaard, J. Prehn, M. B. Nielsen, E. Levillain, M. Allain, J. Becher, *J. Am. Chem. Soc.* **2000**, *122*, 9486–9494.

[34] W. K. Wang, Y. Y. Chen, H. Wang, D. W. Zhang, Y. Liu, Z. T. Li, *Chemistry - An Asian Journal* **2014**, *9*, 1039–1044.

[35] S. V. Rosokha, J. K. Kochi, *J. Am. Chem. Soc.* **2007**, *129*, 828–838.

[36] L. Chen, S. C. Zhang, H. Wang, Y. M. Zhou, Z. T. Li, D. W. Zhang, *Tetrahedron* **2014**, *70*, 4778–4783.

[37] J. Guasch, L. Grisanti, V. Lloveras, J. Vidal-Gancedo, M. Souto, D. C. Morales, M. Vilaseca, C. Sissa, A. Painelli, I. Ratera, C. Rovira, J. Veciana, *Angewandte Chemie International Edition* **2012**, *51*, 11024–11028.

[38] T. Jörgensen, T. K. Hansen, J. Becher, *Chem. Soc. Rev.* **2004**, *23*, 41–51.

[39] F. Gao, F. F. Zhu, X. Y. Wang, Y. Xu, X. P. Wang, J. L. Zuo, *Inorganic Chemistry* **2014**, *53*, 5321–5327.

[40] J. D. Singh, H. B. Singh, *J. Chem. Soc. Perkin Trans. 1* **1992**, 2913–2916.

[41] S. Y. Tan, R. A. Lazenby, K. Bano, J. Zhang, A. M. Bond, J. V. Macpherson, P. R. Unwin, *Phys. Chem. Chem. Phys.* **2017**, *19*, 8726–8734.

[42] P. Day, M. Kurmoo, *J. Mater. Chem.* **1997**, *7*, 1291–1295.

[43] Richard D. Webster, Robert A. W. Dryfe, Barry A. Coles, R. G. Compton, **1998**, DOI `10.1021/AC9708147`.

[44] J. A. Weil, J. R. Bolton, *Electron paramagnetic resonance : elementary theory and practical applications.* Wiley-Interscience, **2007**, p. 664.

[45] A. Neudeck, A. Petr, L. Dunsch, *Synth. Met.* **1999**, *107*, 143–158.

[46] P. Rapta, A. Neudeck, A. Petr, L. Dunsch, *J. Chem. Soc. - Faraday Trans.* **1998**, *94*, 3625–3630.

[47] P. Rapta, J. Lukkari, J. Tarábek, M. Salomäki, M. Jussila, G. Yohannes, M. L. Riekkola, J. Kankare, L. Dunsch, *Phys. Chem. Chem. Phys.* **2004**, *6*, 434–441.

[48] S. Stoll, A. Schweiger, *J. Magn. Reson.* **2006**, *178*, 42–55.

[49] F. Opekar, I. Jelínek, P. Rychlovský, Z. Plzálk, *Základní analytická chemie*, **2003**, p. 106.

[50] F. Scholz, *ChemTexts* **2015**, *1*, 1–24.

[51] D. Z. Goodson in *Math. Methods Phys. Anal. Chem.* John Wiley & Sons, Inc., **2011**, pp. 111–150.

[52] G. Magnettech Company, Quantification of ESR, `https://www.magnettech.de/applications/quantification-of-esr/spin-density-measurement.html`, Online; accessed 14-May-2019.

[53] K. Haubner, J. Tarábek, F. Ziegs, V. Lukeš, E. Jaehne, L. Dunsch, *The Journal of Physical Chemistry A* **2010**, *114*, 11545–11551.